Rotational band structures in ^{127}Cs: Shape changes induced by $h_{11/2}$ neutron alignment

Y. Liang, R. Ma, E. S. Paul,* N. Xu, and D. B. Fossan
Department of Physics, State University of New York at Stony Brook, Stony Brook, New York 11794

R. A. Wyss
The Manne Siegbahn Insitute of Physics, Frescativägen 24, S-104 05 Stockholm 50, Sweden
(Received 5 March 1990)

Several rotational bands have been populated to high spin in ^{127}Cs following the ^{120}Sn(^{11}B,4n) reaction. Rotational bands built on low-lying proton $g_{7/2}$, $d_{5/2}$, and $g_{9/2}$ (hole) orbitals, and the unique-parity $h_{11/2}$ orbital were observed and identified. For the $\pi g_{9/2}$ (hole) case, both signatures were seen in a strongly coupled $\Delta I=1$ band, while for the other cases, decoupled $\Delta I=2$ bands were observed with strong in-band quadrupole transitions. Through comparisons with cranked-shell-model calculations, these band structures are understood to be associated with a prolate ($\gamma\sim 0°$) deformed nuclear shape. At frequencies above $\hbar\omega=0.3$ MeV, the rotational alignment of a pair of $h_{11/2}$ neutrons was observed for each of the $h_{11/2}$, $g_{7/2}$, and $d_{5/2}$ bands. This neutron alignment is predicted to drive the nuclear core away from a prolate shape towards the collectively rotating oblate ($\gamma=-60°$) shape. Changes in the measured signature splittings for the bands below and above the alignment are consistent with the shape changes.

I. INTRODUCTION

There has been considerable interest in the studies of odd-Z nuclei in the $Z>50$ transitional nuclear region. The Cs ($Z=55$) nuclei form an important link in the study of this region from the primarily vibrational Sn ($Z=50$) nuclei to the well deformed La ($Z=57$) and Ce ($Z=58$) nuclei. From the study of these nuclei, an understanding of the potential-energy surfaces and overall nuclear properties as a function of the Fermi surface can be achieved. Earlier measurements (e.g., Ref. 1) led to the conclusion that these nuclei are quite soft to changes in the nuclear shape caused by quasiparticle driving forces.[2,3] Indeed, these nuclei are predicted[4,5] to be soft with respect to γ, the triaxiality parameter in the polar description of rotating quadrupole shapes. In this mass region, the neutron Fermi surface is near the $h_{11/2}$ mid-shell, while the proton Fermi surface is at the bottom of the $h_{11/2}$ shell. Both potential-energy surface (PES) and cranked-shell-model (CSM) calculations suggest that energies of the valence $h_{11/2}$ protons and $h_{11/2}$ neutrons decrease to their deepest minima at $\gamma\sim 0°$ and $\sim -60°$, respectively. Thus the valence $h_{11/2}$ quasiprotons stabilize the nucleus at a prolate ($\gamma\sim 0°$) shape, while the valence $h_{11/2}$ neutrons drive toward the collectively rotating oblate shape ($\gamma\sim -60°$, Lund convention[6]).

For odd-proton nuclei in this γ-soft mass region, the nuclear shape is mainly influenced by the valence quasiproton at low rotational frequencies, while at higher frequencies one needs to consider also the shape-driving effects of additional rotationally aligned quasiparticles. The Coriolis breakup and alignment of pairs of particles in this mass region occurs most easily for particles from the $h_{11/2}$ subshell. For the cesium nuclei, the lowest-frequency rotational alignment is predicted for a pair of $h_{11/2}$ neutrons. As a consequence of the additional driving force induced by the aligned $\nu h_{11/2}$ neutrons, the nucleus is expected to move away from a prolate ($\gamma\sim 0°$) shape to a triaxial ($-60°<\gamma<0°$) or even an oblate ($\gamma\sim -60°$) shape. Some recent results regarding such alignment and shape changes in nuclei of this mass region are discussed in Refs. 1 and 7.

For these odd-proton nuclei, the signature splitting of the band energies is sensitive to the γ deformation. In the case of the $h_{11/2}$ proton band, which is near prolate, there is a large signature splitting, but following the alignment of a pair of $h_{11/2}$ neutrons, the signature splitting decreases as γ is driven toward the oblate shape. The alignment of a pair of $h_{11/2}$ protons, on the other hand, would stabilize the nucleus at $\gamma\sim 0°$ maintaining the large signature splitting. Thus a precise measurement of the signature splitting allows the determination of the type of rotational alignment and the resultant nuclear shape.

Low-lying states in ^{127}Cs, following the β decay of ^{127}Ba, have been reported by Beyer *et al.*,[8] while a γ-γ coincidence experiment was previously performed by Garg *et al.*[9] The current experiment confirms the previous results for the lower-spin states and reveals much more high-spin information. The present paper focuses on the latest experimental results and compares them to recent theoretical predictions, namely deformation self-consistent total-Routhian surface (TRS) cranking calculations.[10]

II. EXPERIMENTAL METHODS AND RESULTS

States in ^{127}Cs were populated using the ^{120}Sn (^{11}B,4$n\gamma$) fusion-evaporation reaction at a bombarding energy of 50 MeV. The ^{11}B beam was provided by the Stony Brook

FN tandem Van de Graaf accelerator. The target consisted of 9.7 mg/cm^2 of isotopically enriched ^{120}Sn rolled onto a lead backing of thickness 100 mg/cm^2, which served to stop the beam particles. The recoiling nuclei were stopped in the target minimizing the Doppler effects. The experiments performed included γ-γ coincidence, γ-ray angular distribution, and pulsed-beam E_γ-t measurements, as discussed below.

A. Coincidence experiments

The γ-γ coincidence data were recorded using an array of five n-type Ge detectors. The detectors were located at angles $+145°$, $+78°$, $-15°$, $-88°$, and $-145°$ with respect to the beam direction. Each Ge detector (efficiency $\sim 25\%$) was surrounded by a transverse bismuth germanate (BGO) shield[11] which served to suppress the Compton background. A coincidence resolving time of $2\tau = 100$ ns was set for the Ge-Ge events. In addition, multiplicity information was recorded using fourteen hexagonal BGO crystals covering a solid angle in excess of 80% of 4π; seven closely packed crystals were positioned above the target chamber and seven below the target chamber. Energy thresholds were set at approximately 100 keV for these BGO crystals, well above the lead x-ray energies. By demanding that at least two or more BGO crystals fired in coincidence with two or more Ge detectors, the radioactivity and Coulomb excitation lines were greatly reduced. With this requirement, approximately 50×10^6 coincidence events were written onto tape event by event.

The data tapes were subsequently scanned offline on a MICROVAX II computer to produce a symmetrized $2k \times 2k$ array of E_γ vs E_γ. Background-subtracted coincidence spectra, extracted from this array, were used in the construction of the level scheme of ^{127}Cs, which is shown in Fig. 1. Examples of such gated spectra are shown in Fig. 2.

An angular correlation array was created from the coincidence data in order to assist in the assignment of multipolarities to the ^{127}Cs transitions. The detectors close to 90° ($+78°$ and $-88°$) were sorted against the other three detectors to produce the two-dimensional angular correlation array, from which it was possible to extract average directional correlation (DCO) intensity ratios.[12] Gates were set on quadrupole transitions along both axes of this array and the intensities of coincident γ rays extracted. Examples of gated spectra obtained from the angle correlation array are shown in Fig. 3. The measured intensity ratios were used to distinguish between stretched dipole and quadrupole transitions. The intensity ratios extracted for stretched quadrupole transitions in

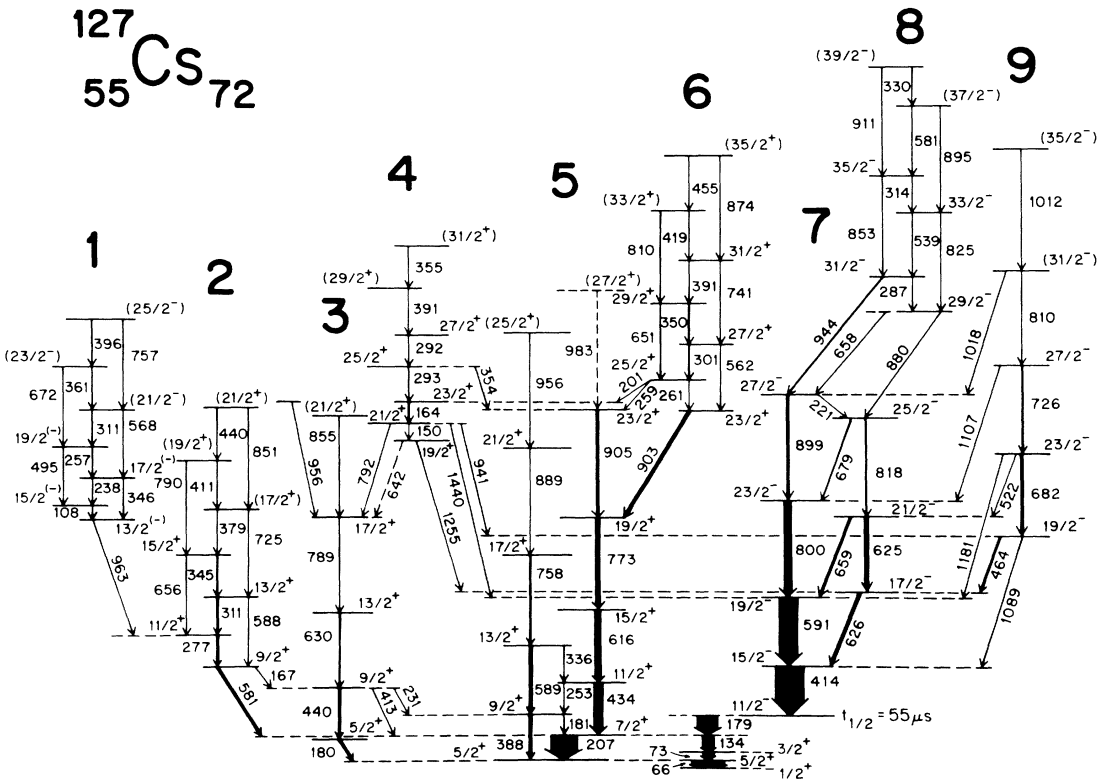

FIG. 1. The decay scheme of ^{127}Cs deduced from this work. The transition energies are given in keV and the widths of the arrows indicate their relative intensities.

this experiment were typically ~ 1.0, while values ≤ 0.6 were obtained for stretched dipole transitions.

B. Angular-distribution data and mixing ratios

A subsequent angular-distribution experiment was performed for the transitions in ^{127}Cs. One Compton-suppressed Ge detector, 22 cm from the target, was placed sequentially at angles 90°, 115°, 125°, 135°, and 145° with respect to the beam axis. A second Ge detector at $-90°$ served as a monitor. The empirical γ-ray intensities were fitted by the formula

$$W(\theta) = A_0 + A_2 P_2(\cos\theta) + A_4 P_4(\cos\theta) , \quad (1)$$

where θ is the detector angle, $P_2(\cos\theta)$ and $P_4(\cos\theta)$ are Legendre polynomials, while A_0, A_2, and A_4 are adjustable parameters. For several $\Delta I = 1$ transitions, the angular-distribution information was used to extract $E2/M1$ mixing ratios. The observed A_2/A_0 and A_4/A_0 coefficients for stretched $E2$ transitions were used to extract average alignment parameters α_2 and α_4; values for α_2 and α_4 were found to be 0.54(11) and 0.72(33), respectively, for band 7, while values of 0.62(21) and 0.70(30) were found for the other bands. These alignment parameters and the experimental angular-

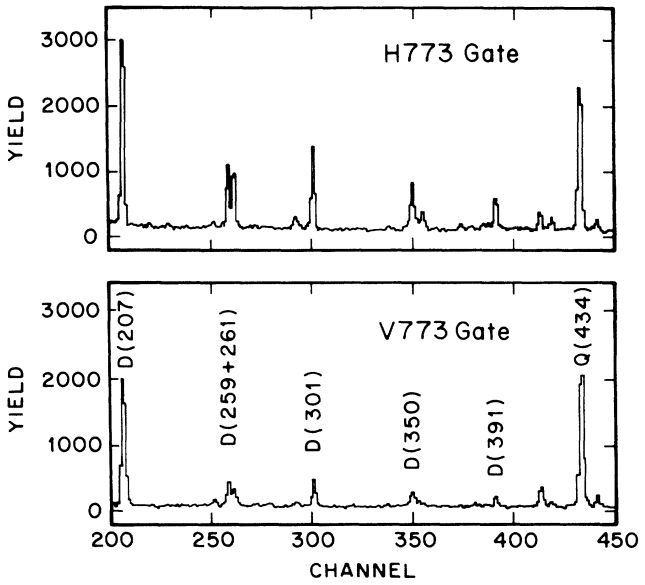

FIG. 3. An example of gated spectra obtained from the angular correlation array. A gate has been set on the 773-keV $\frac{19}{2}^+ \rightarrow \frac{15}{2}^+$ quadrupole transition of band 5. The top spectrum, labeled H773, corresponds to the gate being set on any one of the three detectors farthest from 90°, while the bottom spectrum, labeled V773, corresponds to the gate being set on either of the two detectors close to 90°. Dipole (D) and quadrupole (Q) transitions, labeled by their energies in keV, are clearly distinguished.

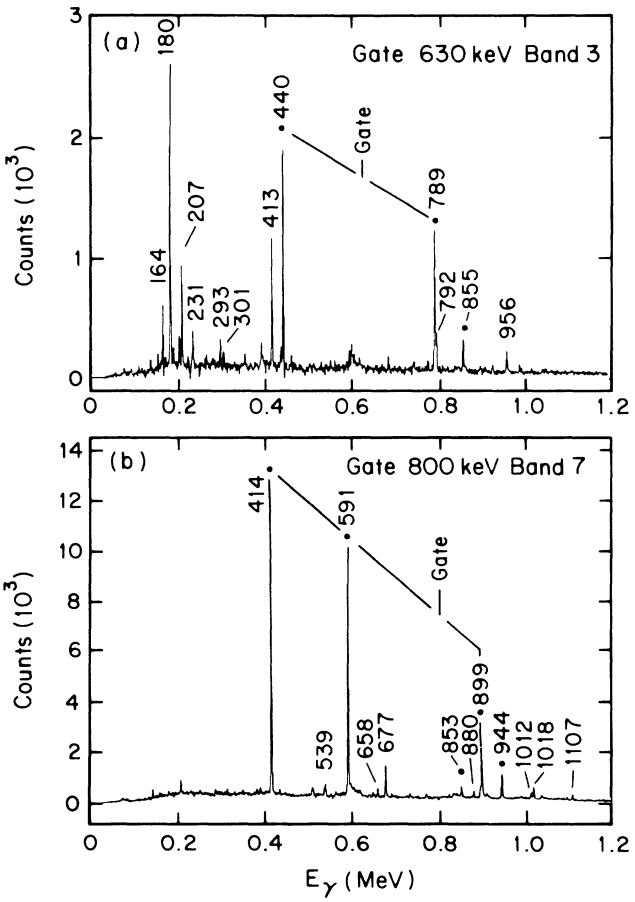

FIG. 2. Examples of gated coincidence spectra. The transition energies are labeled in keV. (a) A gate set on the 630-keV transition of band 3. (b) A gate set on the 800-keV transition of band 7.

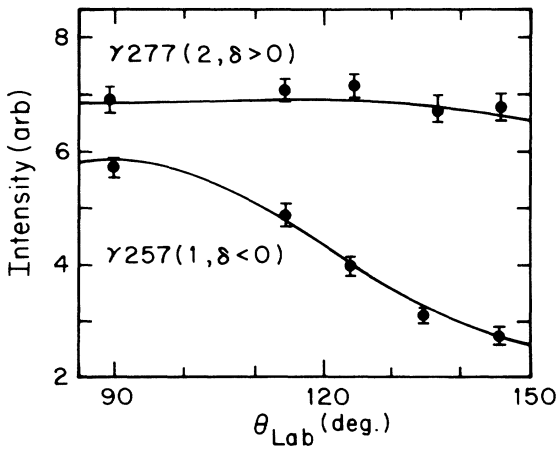

FIG. 4. Angular distributions for dipole transitions of bands 1 and 2. The 257-keV transition of band 1 is found to have a negative $E2/M1$ mixing ratio δ, while that extracted for the 277-keV transition of band 2 is positive.

TABLE I. Energies, relative intensities, and angular-distribution and/or correlation data for transitions assigned to ^{127}Cs following the ^{120}Sn(^{11}B,4$n\gamma$) reaction at 50 MeV.

E_γ[a] (keV)	Relative[b] intensity	A_2/A_0	A_4/A_0	DCO[c] ratio	Mixing ratio mult.[d]	Assignment
65.8[e]	> 100				$E2$[f]	$\frac{5}{2}^+ \rightarrow \frac{1}{2}^+$
72.8[e]	> 50				$M1/E2$[f]	$\frac{3}{2}^+ \rightarrow \frac{5}{2}^+$
108.3	< 2	−0.340(40)	−0.169(57)		$-0.3 < \delta < 0$	$\frac{15}{2}^- \rightarrow \frac{13}{2}^-$
					$M1/E2$	
134.2[e]	40(1)			0.81(2)	$E2$	$\frac{7}{2}^+ \rightarrow \frac{3}{2}^+$
150[g]	< 3	h	h		$M1/E2$	$\frac{21}{2}^+ \rightarrow \frac{19}{2}^+$
163.6	6(4)	−0.336(42)	+0.025(58)		$-0.3 < \delta < 0$	$\frac{23}{2}^+ \rightarrow \frac{21}{2}^+$
					$M1/E2$	
167	< 2				$M1/E2$	$\frac{9}{2}^+ \rightarrow \frac{9}{2}^+$
179.4	72(7)				$M2$	$\frac{11}{2}^- \rightarrow \frac{7}{2}^+$
180	7(1)	h	h	0.96(3)	$M1/E2$	$\frac{5}{2}^+ \rightarrow \frac{5}{2}^+$
181	< 2				$M1/E2$	$\frac{9}{2}^+ \rightarrow \frac{7}{2}^+$
201	3(1)	−0.344(49)	+0.046(67)		−0.14(18)	$\frac{25}{2}^+ \rightarrow \frac{23}{2}^+$
206.9[e]	96(1)			0.73(1)	$M1/E2$	$\frac{7}{2}^+ \rightarrow \frac{5}{2}^+$
220.8	5(1)	+0.130(63)	+0.091(82)		$\delta = +0.28(3)$	$\frac{27}{2}^- \rightarrow \frac{25}{2}^-$
					$M1/E2$	
231	< 2				$M1/E2$	$\frac{9}{2}^+ \rightarrow \frac{9}{2}^+$
237.8	< 2	−0.882(40)	+0.103(63)		$-1.8 < \delta < -0.4$	$\frac{17}{2}^- \rightarrow \frac{15}{2}^-$
					$M1/E2$	
253	< 2				$M1/E2$	$\frac{11}{2}^+ \rightarrow \frac{9}{2}^+$
256.4	< 2	−0.629(53)	+0.174(63)		$-1.6 < \delta < -0.3$	$\frac{19}{2}^- \rightarrow \frac{17}{2}^-$
					$M1/E2$	
259.5	3(1)	−0.458(48)	+0.114(67)		$-1.2 < \delta < -0.1$	$\frac{25}{2}^+ \rightarrow \frac{23}{2}^+$
					$M1/E2$	
261.4	3(1)	−0.611(51)	+0.193(71)	0.36(2)	$-1.8 < \delta < -0.2$	$\frac{25}{2}^+ \rightarrow \frac{23}{2}^+$
					$M1/E2$	
277.1	8(1)	−0.055(44)	−0.046(58)		$\delta = +0.11(6)$	$\frac{11}{2}^+ \rightarrow \frac{9}{2}^+$
					$M1/E2$	
287	< 2			0.59(7)	$M1/E2$	$\frac{31}{2}^- \rightarrow \frac{29}{2}^-$
292					$\delta = -0.23(20)$	$\frac{27}{2}^+ \rightarrow \frac{25}{2}^+$
292.5	5(1)	−0.440(46)	+0.054(64)		$M1/E2$	$\frac{25}{2}^+ \rightarrow \frac{23}{2}^+$
301.4	7(1)	−0.551(38)	+0.007(5)	0.39(3)	$\delta = -0.24(17)$	$\frac{27}{2}^+ \rightarrow \frac{25}{2}^+$
					$M1/E2$	
311.0	5(1)	h	h		$M1/E2$	$\frac{13}{2}^+ \rightarrow \frac{11}{2}^+$
311.7	< 2				$M1/E2$	$(\frac{21}{2}^-) \rightarrow \frac{19}{2}^{(-)}$
314	< 2			0.41(8)	$M1/E2$	$\frac{35}{2}^- \rightarrow \frac{33}{2}^-$
330	< 2				$M1/E2$	$(\frac{39}{2}^- \rightarrow \frac{37}{2}^-)$
336	< 2				$M1/E2$	$\frac{13}{2}^+ \rightarrow \frac{11}{2}^+$
345.6	3(1)	−0.048(56)	−0.007(73)		$\delta = +0.11(1)$	$\frac{15}{2}^+ \rightarrow \frac{13}{2}^+$
					$M1/E2$	
346	< 2				$E2$	$\frac{17}{2}^- \rightarrow \frac{13}{2}^-$
350.2	4(1)	−0.473(39)	+0.093(55)	0.31(1)	$-1.2 < \delta < -0.1$	$\frac{29}{2}^+ \rightarrow \frac{27}{2}^+$
					$M1/E2$	
354	< 2				$M1/E2$	$\frac{25}{2}^+ \rightarrow \frac{23}{2}^+$
355	< 2				$(M1/E2)$	$(\frac{31}{2}^+ \rightarrow \frac{29}{2}^+)$
361.6	< 2				$(M1/E2)$	$(\frac{23}{2}^- \rightarrow \frac{21}{2}^-)$
379	< 2				$(M1/E2)$	$(\frac{17}{2}^+) \rightarrow \frac{15}{2}^+$
388.8	14(1)	+0.108(46)	−0.061(56)	0.98(4)	$E2$	$\frac{9}{2}^+ \rightarrow \frac{5}{2}^+$
391	< 2				$(M1/E2)$	$(\frac{29}{2}^+) \rightarrow \frac{27}{2}^+$
391.6	< 3	−0.525(48)	+0.075(68)	0.45(50)	$-0.9 < \delta < -0.3$	$\frac{31}{2}^+ \rightarrow \frac{29}{2}^+$
					$M1/E2$	
396.2	< 2				$(M1/E2)$	$(\frac{25}{2}^- \rightarrow \frac{23}{2}^-)$
411	< 2				$(M1/E2)$	$(\frac{19}{2}^+ \rightarrow \frac{17}{2}^+)$

TABLE I. (*Continued*).

E_γ[a] (keV)	Relative[b] intensity	A_2/A_0	A_4/A_0	DCO[c] ratio	Mixing ratio mult.[d]	Assignment
413	<2				$M1/E2$	$\frac{9}{2}^+ \rightarrow \frac{7}{2}^+$
413.9	≡100	+0.146(50)	−0.082(60)	1.03(2)	$E2$	$\frac{15}{2}^- \rightarrow \frac{11}{2}^-$
419	<2				$(M1/E2)$	$(\frac{33}{2}^+) \rightarrow \frac{31}{2}^+$
434.2	30(1)	+0.141(46)	−0.090(56)	1.00(1)	$E2$	$\frac{11}{2}^+ \rightarrow \frac{7}{2}^+$
439.3	7(1)	+0.113(48)	−0.052(59)	1.01(3)	$E2$	$\frac{9}{2}^+ \rightarrow \frac{5}{2}^+$
440	<2				$(M1/E2)$	$(\frac{21}{2}^+ \rightarrow \frac{19}{2}^+)$
455	<2				$(M1/E2)$	$(\frac{35}{2}^+ \rightarrow \frac{33}{2}^+)$
464.4	8(1)	−0.696(38)	+0.139(54)		$\delta = -0.84(28)$	$\frac{19}{2}^- \rightarrow \frac{17}{2}^-$
					$M1/E2$	
495	<2				$E2$	$\frac{19}{2}^- \rightarrow \frac{15}{2}^-$
522.2	5(1)	−0.706(44)	+0.138(62)		$\delta = -0.89(30)$	$\frac{23}{2}^- \rightarrow \frac{21}{2}^-$
					$M1/E2$	
539	<2			0.38(4)	$M1/E2$	$\frac{33}{2}s \rightarrow \frac{31}{2}^-$
568	<2				$(E2)$	$(\frac{21}{2}^-) \rightarrow \frac{17}{2}^-$
581.1	13(1)	+0.033(46)	+0.036(59)		$\delta = +0.19(2)$	$\frac{9}{2}^+ \rightarrow \frac{7}{2}^+$
					$M1/E2$	
588	2				$E2$	$\frac{13}{2}^+ \rightarrow \frac{9}{2}^+$
589	13(1)	h	h	0.99(5)	$E2$	$\frac{13}{2}^+ \rightarrow \frac{9}{2}^+$
591.1	66(1)	+0.241(50)	−0.128(60)	1.07(1)	$E2$	$\frac{19}{2}^- \rightarrow \frac{15}{2}^-$
615.9	25(1)	+0.280(50)	−0.132(58)	1.06(2)	$E2$	$\frac{15}{2}^+ \rightarrow \frac{11}{2}^+$
625.7	12(1)	h	h		$E2$	$\frac{21}{2}^- \rightarrow \frac{17}{2}^-$
626.3	15(1)	h	h		$M1/E2$	$\frac{17}{2}^- \rightarrow \frac{15}{2}^-$
630.1	6(1)	+0.203(54)	+0.039(67)	0.98(4)	$E2$	$\frac{13}{2}^+ \rightarrow \frac{9}{2}^+$
642	<2				$M1/E2$	$\frac{19}{2}^+ \rightarrow \frac{17}{2}^+$
651	<2				$E2$	$\frac{29}{2}^+ \rightarrow \frac{25}{2}^+$
656	<2				$E2$	$\frac{15}{2}^+ \rightarrow \frac{11}{2}^+$
658	<2			0.61(6)	$M1/E2$	$\frac{29}{2}^- \rightarrow \frac{27}{2}^-$
659.2	12(1)	−0.865(36)	+0.144(50)	0.25(3)	$\delta = -0.70(5)$	$\frac{21}{2}^- \rightarrow \frac{19}{2}^-$
					$M1/E2$	
672	<2				$(E2)$	$(\frac{23}{2}^-) \rightarrow \frac{19}{2}^-$
679	5(1)	−0.661(45)	+0.276(63)	0.20(6)	$\delta = -1.10(78)$	$\frac{25}{2}^- \rightarrow \frac{23}{2}^-$
					$M1/E2$	
682.4	11(1)	+0.256(50)	−0.144(60)	1.08(4)	$E2$	$\frac{23}{2}^- \rightarrow \frac{19}{2}^-$
725	2				$(E2)$	$(\frac{17}{2}^+) \rightarrow \frac{13}{2}^+$
726.8	8(1)	+0.152(51)	−0.041(63)	0.96(8)	$E2$	$\frac{27}{2}^- \rightarrow \frac{23}{2}^-$
741	<2					$\frac{31}{2}^+ \rightarrow \frac{27}{2}^+$
757	<2				$(E2)$	$(\frac{25}{2}^- \rightarrow \frac{21}{2}^-)$
758.7	6(1)	+0.309(60)	+0.003(73)	1.05(6)	$E2$	$\frac{17}{2}^+ \rightarrow \frac{13}{2}^+$
773.1	23(1)	+0.251(49)	−0.129(57)	1.05(2)	$E2$	$\frac{19}{2}^+ \rightarrow \frac{15}{2}^+$
788.6	3(1)	+0.285(59)	−0.154(73)	0.88(3)	$E2$	$\frac{17}{2}^+ \rightarrow \frac{13}{2}^+$
790	<2				$(E2)$	$(\frac{19}{2}^+) \rightarrow \frac{15}{2}^+$
792	<2			0.97(10)	$E2$	$\frac{21}{2}^+ \rightarrow \frac{17}{2}^+$
800.2	31(1)	+0.214(50)	−0.115(57)	1.10(1)	$E2$	$\frac{23}{2}^- \rightarrow \frac{19}{2}^-$
810					$(E2)$	$(\frac{31}{2}^-) \rightarrow \frac{27}{2}^-$
810	<2				$(E2)$	$(\frac{33}{2}^+) \rightarrow \frac{29}{2}^+$
818.0	7(1)	+0.151(51)	−0.048(63)		$E2$	$\frac{25}{2}^- \rightarrow \frac{21}{2}^-$
825	<2				$E2$	$\frac{33}{2}^- \rightarrow \frac{29}{2}^-$
851	<2				$(E2)$	$(\frac{21}{2}^+ \rightarrow \frac{17}{2}^+)$
853	<2			0.85(5)	$E2$	$\frac{35}{2}^- \rightarrow \frac{31}{2}^-$
855	<2				$(E2)$	$(\frac{21}{2}^+) \rightarrow \frac{17}{2}^+$
874	<2				$(E2)$	$(\frac{35}{2}^+) \rightarrow \frac{31}{2}^+$
880.1	3(1)	+0.139(94)	0.040(91)	0.91(5)	$E2$	$\frac{29}{2}^- \rightarrow \frac{25}{2}^-$

TABLE I. (*Continued*).

E_γ[a] (keV)	Relative[b] intensity	A_2/A_0	A_4/A_0	DCO[c] ratio	Mixing ratio mult.[d]	Assignment
888.9	3(1)	+0.306(75)	−0.072(95)	1.01(10)	$E2$	$\frac{21}{2}^+ \rightarrow \frac{17}{2}^+$
895	<2				$(E2)$	$(\frac{37}{2}^-) \rightarrow \frac{33}{2}^-$
898.5	12(1)	+0.205(49)	−0.109(59)	1.03(2)	$E2$	$\frac{27}{2}^- \rightarrow \frac{23}{2}^-$
903.4	8(1)	+0.141(49)	−0.107(61)	1.10(3)	$E2$	$\frac{23}{2}^+ \rightarrow \frac{19}{2}^+$
905.5	5(1)	+0.211(53)	−0.134(63)	1.11(4)	$E2$	$\frac{23}{2}^+ \rightarrow \frac{19}{2}^+$
911					$(E2)$	$(\frac{39}{2}^-) \rightarrow \frac{35}{2}^-$
941	<2				$E1$	$\frac{21}{2}^+ \rightarrow \frac{19}{2}^-$
944.4	6(1)	+0.120(57)	+0.030(72)	1.03(5)	$E2$	$\frac{31}{2}^- \rightarrow \frac{27}{2}^-$
956					$(E2)$	$(\frac{25}{2}^+) \rightarrow \frac{21}{2}^+$
956	<2					$\rightarrow \frac{17}{2}^+$
963.2	2.5(4)	−0.200(58)	−0.030(82)		$\delta=0.00(3)$ $E1$	$\frac{13}{2}^- \rightarrow \frac{11}{2}^+$
983	<2				$(E2)$	$(\frac{27}{2}^+) \rightarrow \frac{23}{2}^+$
1012	<2				$(E2)$	$(\frac{35}{2}^- \rightarrow \frac{31}{2}^-)$
1018	<2				$(E2)$	$(\frac{31}{2}^-) \rightarrow \frac{27}{2}^-$
1088.9	4(1)	+0.270(62)	−0.026(76)	0.90(4)	$E2$	$\frac{19}{2}^- \rightarrow \frac{15}{2}^-$
1107				0.91(3)	$E2$	$\frac{27}{2}^- \rightarrow \frac{23}{2}^-$
1180	<3			0.83(9)	$E2$	$\frac{23}{2}^- \rightarrow \frac{19}{2}^-$
1255.5	<3	−0.100(98)	≡0		$E1$	$\frac{19}{2}^+ \rightarrow \frac{17}{2}^-$
1440	<2				$M1/E2$	$\frac{21}{2}^+ \rightarrow \frac{19}{2}^-$

[a]Gamma-ray energies are accurate to ±0.3 keV, except those quoted as integers which are accurate to ±1.0 keV.
[b]Transition intensities were obtained from a combination of singles and coincidence data, and are normalized to the 413.9-keV $\frac{15}{2}^- \rightarrow \frac{11}{2}^-$ transition.
[c]DCO ratios observed are typically ≥ 1.0 for stretched quadrupole transitions, and ≤0.6 for stretched dipole transitions.
[d]Multipolarity of the gamma rays observed.
[e]Transition below the $\frac{11}{2}^-$ isomer which has a half-life $t_{1/2}=55$ μs.
[f]Multipolarity taken from Ref. 8.
[g]Doublet with a transition in ^{128}Cs.
[h]Unresolved doublet transition.

distribution coefficients were combined with the theoretical angular-distribution functions from Ref. 13 to extract the $E2/M1$ mixing ratios δ; a χ^2 minimization technique was employed.[14] The results of this analysis are included in Table I where the sign convention of Ref. 13 has been adopted. In addition, Fig. 4 compares the angular-distribution results for the 257-keV transition of band 1 ($\delta<0$) and the 277-keV transition band 2 ($\delta>0$).

The results of the angular-distribution and angular correlation measurements are presented in Table I together with the relative intensities of all the transitions assigned to ^{127}Cs; the relative intensities, corrected for detector efficiency and internal conversion effects, were obtained from a combination of singles and coincidence spectra.

C. Lifetime data

A pulsed-beam E_γ-t measurement was performed in order to search for high-spin isomeric states in ^{127}Cs. The pulsed beam of the Stony Brook LINAC was utilized with 106 ns between successive beam pulses. The ^{120}Sn(^{11}B,4n)^{127}Cs reaction was repeated using the tandem Van de Graaf accelerator to inject the LINAC. A standard delayed-coincidence technique was used for the measurement of short lifetimes (ns). The distribution of time delays between the arrival of the beam and subsequent decay of γ rays was recorded event by event onto magnetic tape. Both a coaxial Ge(Li) detector and a Compton-suppressed Ge detector were used to mark the decay times and record the γ-ray energies. However, except for known low-lying isomeric $\frac{11}{2}^-$ and $\frac{5}{2}^+$ states, no half-lives greater than 8 ns were observed in ^{127}C.

D. The level scheme of ^{127}Cs

The decay scheme for ^{127}Cs, deduced from the present study, is shown in Fig. 1. The levels have been arranged into several bands labeled 1–9 in order to facilitate the discussion. The ordering of the γ rays has been determined by coincidence relationships and relative intensities. For some weak transitions, the placement in the level scheme is uncertain; these transitions are shown dashed. Spins and parities of the levels were assigned on the basis of angular-distribution and correlation measurements together with the systematics from neighboring

odd-Z nuclei. The ground state of $\frac{1}{2}^+$ and the first $\frac{3}{2}^+$, $\frac{5}{2}^+$, and $\frac{7}{2}^+$ states were assigned by previous measurements.[8] The first few transitions of band 5 and band 7 were known from earlier studies by Garg *et al.*;[9] the other band structures were established for the first time.

Based upon the multipolarities of the γ transitions, the spin and parity assignments are straightforward. Assignments for band 3 were based on the multipolarities of the 180-keV and 413-keV linking transitions, which feed into $\frac{5}{2}^+$ and $\frac{7}{2}^+$ states, respectively. The DCO ratios obtained for the 413-keV and 180-keV transitions are 0.63(2) and 0.96(3). Taking into consideration the $E2$ multipolarity (DCO ratio $\sim$1.0) for the 440-keV in-band transition in band 3, the results indicate a stretched dipole character for the 413-keV transition and a nonstretched dipole character for the 180-keV transition. Therefore $I^\pi=\frac{5}{2}^+$ is assigned to the lowest state of band 3 at 246 keV. A comparison with the nearby odd-Z ^{131}La nucleus,[15] where a similar band has been found built on a $\frac{5}{2}^+$ state, supports this assignment.

Band 5 includes two sequences of $\Delta I=2$ $E2$ transitions connected by weaker $\Delta I=1$ transitions. The $\frac{5}{2}^+$ bandhead at 66 keV and the $\frac{7}{2}^+$ band member at 273 keV have previously been established from β-decay characteristics and internal conversion measurements.[8] The $\frac{5}{2}^+$ state at 66 keV is isomeric with a half-life $t_{1/2}=24.5(\pm3)$ ns. Bands showing similar properties (energies, bandhead spins, and decay patterns) have been reported in other nearby odd-proton nuclei.[15–17]

The negative-parity band 7 also includes two sets of $\Delta I=2$ sequences. The first sequence built on the $\frac{11}{2}^-$ state is yrast, therefore, it was strongly populated in the present reaction. The second $\Delta I=2$ sequence, which includes the 625- and 818-keV transitions, was observed for the first time in the present experiment. The results of the angular-distribution analysis indicate that both the 659- and 679-keV γ rays, which connect the two $\Delta I=2$ sequences, are stretched dipole transitions. Thus $I^\pi=\frac{17}{2}^-$ was assigned to the lowest state of the second sequence, and the linking transitions have been interpreted as mixed $M1/E2$ transitions. For band 7, the bandhead is an $\frac{11}{2}^-$ isomeric state, which connects to the $\frac{7}{2}^+$ state via a 179-keV $M2$ transition. The half-life of the $\frac{11}{2}^-$ level has been measured by Conlon[18] as $t_{1/2}=55(\pm3)$ μs. Because of the long half-life, no coincidences were observed between the transitions occurring above and below the isomer.

Band 8 is the direct extension of band 7. The DCO ratios and A_2/A_0 coefficients obtained for both the 944- and 880-keV transitions are consistent with stretched quadrupole assignments. Unlike the dominating $\Delta I=2$ decay sequences in band 7, the $\Delta I=1$ $M1/E2$ transitions become as strong as the crossover $\Delta I=2$ $E2$ transitions in band 8. This band was observed up to $I^\pi=(\frac{39}{2}^-)$.

Band 9 was weakly populated in the present experiment. The information on the multipolarity of the transitions involved could only be obtained for a few resolved cases. Because of the observed systematic decays to the yrast sequence, a consistent set of negative-parity levels is defined for this $\Delta I=2$ band. A characteristic feature of band 9 is that the intensity of the in-band $E2$ transition from each level is weak compared to that of the branching transitions out of the band. Based on the A_2/A_0 coefficients of +0.270(62) for the 1089-keV transition and −0.696(38) for the 464-keV transition from the bandhead, the decay pattern for most of the band members is interpreted as involving stretched $E2$ ($\Delta I=2$) and mixed $M1/E2$ ($\Delta I=1$) transitions to the two $\Delta I=2$ sequences of band 7.

A particularly interesting aspect of the present study is the observation of several $\Delta I=1$ bands where the dipole transitions dominate and the crossover quadrupole transitions were either weakly observed (bands 1, 2, and 6) or not observed (band 4). Several members of band 4 exhibit angular distributions characteristic of mixed $M1/E2$ $\Delta I=1$ transitions. This band decays to band 3 via a 792-keV transition. The DCO ratio obtained for this transition is 0.97(10), implying an $E2$ multipolarity. Thus $I^\pi=\frac{19}{2}^+$ has been assigned to the bandhead of band 4. Band 6 also shows strong $\Delta I=1$ in-band transitions while the $E2$ crossovers were observed only weakly. The large negative A_2/A_0 coefficients for the $\Delta I=1$ γ rays indicate mixed $M1/E2$ transitions with $E2/M1$ mixing ratios $\delta<0$. The decay pattern from band 6 to band 5 involves a 903-keV $E2$ transition and a 259-keV $M1/E2$ transition. A third $\Delta I=1$ band, labeled 2 in Fig. 1, feeds into the $\frac{7}{2}^+$ state via a 581-keV transition. The small A_2/A_0 coefficient found for the 581-keV transition implies a mixed $M1/E2$ transition with a positive mixing ratio $\delta>0$. Thus $I^\pi=\frac{9}{2}^+$ was assigned to the bandhead of band 2. This newly observed band extends the systematics found previously for similar proton-hole bands in the $^{119-125}$Cs isotopes.[19] The spin and parity assignment for band 1 was directly based on the multipolarity of the 963-keV transition. The A_2/A_0 coefficient for this linking transition was found to be −0.200(58), while the extracted mixing ratio δ is 0.00(3). These results imply a pure stretched dipole transition. With a consideration of possible quasiparticle configurations, we conclude that the 963-keV transition is most likely a $\Delta I=1$ $E1$ transition. Thus negative parity was tentatively assigned to band 1.

III. DISCUSSION

In order to discuss the rotational properties of the bands shown in Fig. 1, experimental alignments are plotted in Fig. 5 for several of the bands as a function of rotational frequency. The alignment is defined as[20]

$$i_x(\omega)=I_x(\omega)-I_{x,\mathrm{ref}}(\omega)\ , \tag{2}$$

where I_x is estimated as $I_x=[(I+\frac{1}{2})^2-K^2]^{1/2}$ and $I_{x,\mathrm{ref}}$ is based on a frequency-dependent moment of inertia reference: $\mathcal{J}_{\mathrm{ref}}=\mathcal{J}_0+\omega^2\mathcal{J}_1$. The Harris parameters[21] for the reference were taken as $\mathcal{J}_0=11.2\hbar^2$ MeV^{-1} and $\mathcal{J}_1=31.2\hbar^4$ MeV^{-3}, respectively. Configurations for the nine band structures, labeled in Fig. 1, are discussed in the following sections, while Table II summarizes the proposed quasiparticle structures associated with each

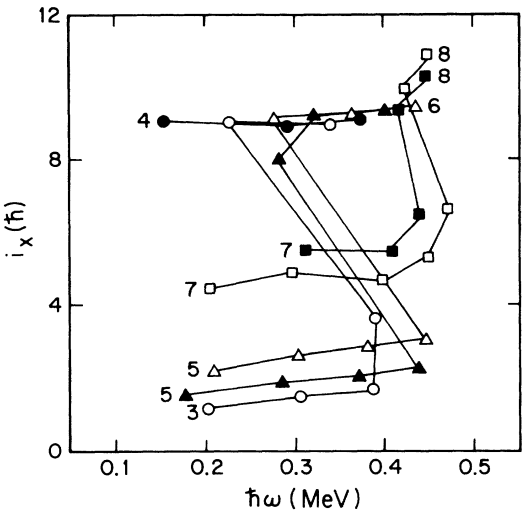

FIG. 5. Experimental alignments for the positive-parity bands 3,4 (circles), 5,6 (triangles), and negative-parity bands 7,8 (squares) in ^{127}Cs shown as a function of rotational frequency. The same symbol is used for the two related signatures, an open symbol for the favored signature and a closed symbol for the unfavored signature.

band.

Deformation self-consistent cranking calculations,[10] based on a universal Woods-Saxon single-particle potential,[22] have been performed for this nucleus. Results are presented in Fig. 6 for the lowest positive- and negative-parity orbitals, labeled by parity and signature quantum numbers (π,α). Figure 6 shows total-Routhian surfaces calculated at rotational frequencies of $\hbar\omega=0.30$ and 0.42 MeV, corresponding to single- and three-quasiparticle configurations, respectively. The single-quasiparticle configurations can be associated with $\pi g_{7/2}$ and $\pi h_{11/2}$ orbitals, while the three-quasiparticle configurations also include rotationally aligned $h_{11/2}$ neutrons. These TRS calculations, which predict the nuclear shape (β_2,γ) for various configurations as a function of rotational frequency, will be discussed in more detail in the following sections.

TABLE II. Quasiparticle assignments for the band structures observed in ^{127}Cs, as shown in Fig. 1.

Band	(π,α)	Configuration
1	$(-,\pm\frac{1}{2})$	$\pi g_{7/2}\otimes\nu h_{11/2}\otimes\nu g_{7/2}$
2	$(+,\pm\frac{1}{2})$	$\pi g_{9/2}$
3	$(+,+\frac{1}{2})$	$\pi d_{5/2}$
4	$(+,\pm\frac{1}{2})$	$\pi d_{5/2}\otimes[\nu h_{11/2}]^2$
5	$(+,\pm\frac{1}{2})$	$\pi g_{7/2}$
6	$(+,\pm\frac{1}{2})$	$\pi g_{7/2}\otimes[\nu h_{11/2}]^2$
7	$(-,\pm\frac{1}{2})$	$\pi h_{11/2}$
8	$(-,\pm\frac{1}{2})$	$\pi h_{11/2}\otimes[\nu h_{11/2}]^2$
9	$(-,-\frac{1}{2})$	$(\pi h_{11/2}\otimes\gamma$ − vib.)

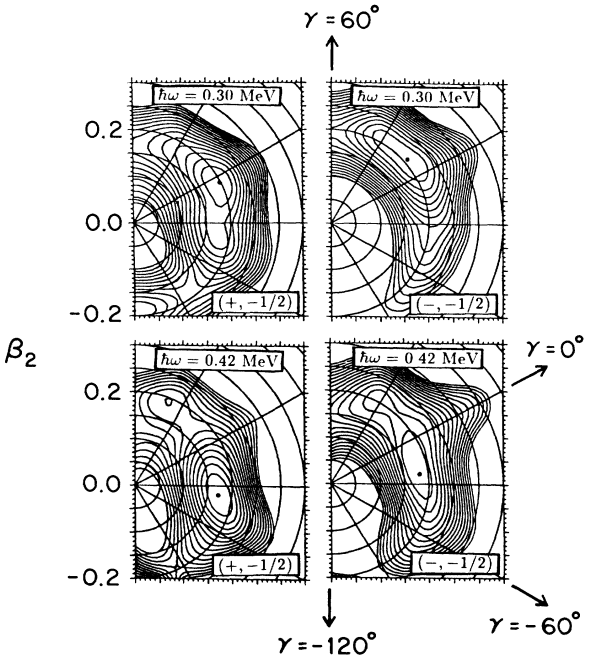

FIG. 6. Total-Routhian-surface calculations for the lowest positive- and negative-parity configurations in ^{127}Cs. The plots are labeled by parity and signature quantum numbers (π,α) and correspond to rotational frequencies $\hbar\omega=0.30$ MeV and $\hbar\omega=0.42$ MeV, respectively.

A. Negative-parity single-quasiproton bands

In this section, interpretations are given for the negative-parity bands 7 and 9, as shown to the right side of Fig. 1.

1. Band 7: $\pi h_{11/2}$ band

Band 7 is associated with the $\pi h_{11/2}$ $[550]\frac{1}{2}^-$ unique-parity orbital. The two $\Delta I=2$ sequences correspond to the two signature components built on the favored $(\alpha=-\frac{1}{2})$ signature ($\frac{11}{2}^-$ bandhead) and the unfavored $(\alpha=+\frac{1}{2})$ signature. The alignments i_x extracted for both signatures are included in Fig. 5. It shows an upbend (band 8) for frequencies above $\hbar\omega=0.40$ MeV which can be attributed to the rotational alignment of a pair of $h_{11/2}$ neutrons, as the $[h_{11/2}]^2$ proton alignment is blocked. The energy difference between the two signatures of band 7, the signature splitting, is approximately 300 keV. This large signature splitting between the two components is expected for the low-Ω $\pi h_{11/2}$ orbital at a prolate shape.

From the measured intensities of the in-band $E2$ transitions and of the $\Delta I=1$ linking transitions,

$$B(M1;I\rightarrow I-1)/B(E2;I\rightarrow I-2)$$

ratios of reduced transition probabilities were extracted for both favored $(\alpha=-\frac{1}{2})$ and unfavored $(\alpha=+\frac{1}{2})$ signatures of the $\pi h_{11/2}$ band, with the measured $E2/M1$ mixing ratios taken into account. The results are shown in Fig. 7 together with the $E2/M1$ mixing ratios obtained

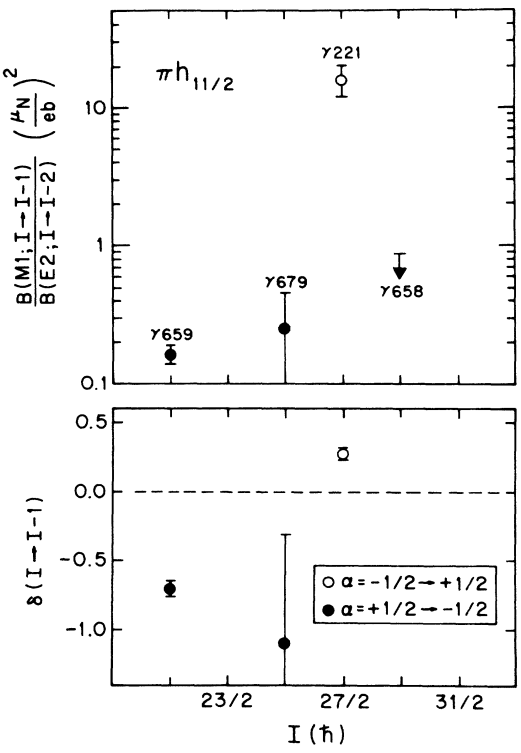

FIG. 7. Experimental ratios of $B(M1)/B(E2)$ reduced transition probabilities and $E2/M1$ mixing ratios δ associated with the yrast $\pi h_{11/2}$ (band 7) shown as a function of spin.

for some of $\Delta I=1$ transitions. The $B(M1)/B(E2)$ ratios exhibit a clear signature dependence with the ratios for the favored to unfavored ($f\rightarrow u$) signature being an order of magnitude larger than the corresponding ratios for the unfavored to favored ($u\rightarrow f$) signature. The $E2/M1$ mixing ratios for the $\Delta I=1$ linking transitions also appear to exhibit a signature dependence; δ was found to be positive for the 221-keV $\frac{27}{2}^-\rightarrow\frac{25}{2}^-$ ($f\rightarrow u$) transition, while negative values were extracted for the 659-keV $\frac{21}{2}^-\rightarrow\frac{19}{2}^-$ and 679-keV $\frac{25}{2}^-\rightarrow\frac{23}{2}^-$ ($u\rightarrow f$) transitions.

$B(M1)/B(E2)$ ratios of a similar magnitude are also extracted for the $\pi h_{11/2}$ band in ^{131}La.[15] These experimental ratios are difficult to reproduce theoretically. The geometrical model of Dönau and Frauendorf[23] underestimates the ratios by two orders of magnitude for a single rotationally aligned $h_{11/2}$ proton occupying the $[550]\frac{1}{2}^-$ orbital in a prolate nucleus ($\gamma=0°$). However, because of the γ-driving forces of the $h_{11/2}$ proton on the γ-soft core, the $h_{11/2}$ configuration may not be axially symmetric, but possess a degree of triaxiality. A triaxial shape would mix higher Ω components into the wave function leading to a higher K value. In addition, the $E2$ transition rates would be decreased for a triaxial shape with a positive value of γ.[24] Taking into account both effects stated above, the $B(M1)/B(E2)$ ratios, which are proportional to $K^2/\cos^2(30°+\gamma)$, would increase and be consistent with the experimental measurements. The TRS calculations, discussed in more detail below, indeed do predict triaxial shapes with positive γ values for the two signatures of the $\pi h_{11/2}$ orbital. The experiment which shows these triaxial properties thus supports the TRS prediction. The model of Dönau and Frauendorf can also predict the $E2/M1$ mixing ratios δ for the $\Delta I=1$ transitions. In particular, if the signature splitting is large enough (here the splitting is $\sim$300 keV at $\hbar\omega=300$ keV), then the mixing ratios are predicted to alternate in sign for consecutive $\Delta I=1$ transitions. The positive value for 221 keV ($f\rightarrow u$) and negative values for 659 and 679 keV ($u\rightarrow f$), shown in Fig. 7, qualitatively support the model predictions.

TRS calculations have been performed in order to predict the nuclear shape (β_2,γ) for the $\pi h_{11/2}$ configuration. These calculations predict a shape $(\beta_2=0.21,\gamma=+12°)$ for the favored $(-,-\frac{1}{2})$ signature and a shape $(\beta_2=0.21,\gamma=-7°)$ for the unfavored signature. It is interesting to note that different shapes are predicted for the two signatures. This is related to the different driving forces of the signature partners of the $h_{11/2}$ protons. Whereas the favored signature clearly prefers positive γ values, the unfavored signature has only a weak γ dependence. Such differences in shape are expected for all soft nuclei, where the valence particle occupies the high-j, low-Ω orbitals which have strong γ-driving forces. The influence of such different triaxial shapes on the $B(M1)/B(E2)$ ratios has not been carefully studied theoretically as yet. Further studies of the $B(M1)/B(E2)$ ratios and $E2/M1$ mixing ratios would help the understanding of these shape dependences.

2. *Band 9*

Bands similar to band 9 have recently been established in odd-Z ^{131}La (Ref. 15) and ^{133}Pr.[16] The characteristic decay patttern of these bands is that each band member has a strong $E2$ branch to the favored signature members of band 7. The most probable explanation is that band 9 is built on an $h_{11/2}$ proton coupled to the γ-vibrational band of the γ-soft core. Similarly, in a triaxial nucleus, one would expect to observe a band built on each state of the rotational sequence. The occurrence of the second $h_{11/2}$ proton band might thus be a further indication of triaxiality in this nucleus. The observation is also in accordance with the low-lying and strongly populated γ-vibrational bands in the neighboring even-even ^{126}Xe (Ref. 25) and ^{128}Ba (Ref. 26) nuclei.

B. Positive-parity single-quasiproton bands

In this section, the decoupled bands 3 and 5 are discussed, together with the strongly coupled band 2.

1. *Band 5: $\pi g_{7/2}$ band*

By consideration of Nilsson single-particle systematics for a prolate deformation $\beta_2\sim0.2$, band 5 is expected to be associated with the two signatures of the $\pi g_{7/2}$ $[422]\frac{3}{2}^+$ orbital. The TRS calculations predict a near prolate $(\beta_2=0.20,\gamma=-3°)$ shape for both signatures of this orbital. The tentative 983-keV transition placed at

the top of band 5 may represent the start of an upbend caused by $h_{11/2}$ proton alignment. Indeed such prolate decoupled $\pi g_{7/2}\otimes[\pi h_{11/2}]^2$ bands have been established in nearby odd-Z lanthanum isotopes, including ^{129,131}La.[27,15]

2. Band 3: $\pi d_{5/2}$ band

Again from Nilsson single-particle systematics, band 3 is believed to be associated with the favored $(+,+\frac{1}{2})$ signature of the $\pi d_{5/2}[420]\frac{1}{2}^+$ orbital. The $\frac{1}{2}^+$ ground state may be part of this band, with the low-lying $\frac{3}{2}^+$ state being the lowest member of the unfavored $(+,-\frac{1}{2})$ signature.

3. Band 2: $\pi g_{9/2}$ proton-hole band

Band 2 is built on a $\frac{9}{2}^+$ state and decays predominantly by in-band $\Delta I=1$ transitions. The $E2/M1$ mixing ratios δ could only be extracted for the 277-keV and the 345-keV transitions; positive values were found. Band 2 shows no signature splitting, consistent with a high-K configuration. Indeed, by comparison with similar bands observed[28,29,19] in light Sb, I, and Cs isotopes, band 2 is associated with the $\pi g_{9/2}$ $[404]\frac{9}{2}^+$ proton-hole orbital from below the $Z=50$ shell closure. The prolate shape, together with the positive g factor for the $\pi g_{9/2}$ quasiparticle, are responsible for the positive mixing ratios δ.

Systematics of the $\frac{9}{2}^+$ bandheads are shown in Fig. 8 for the series of odd-Z cesium isotopes from ^{119}Cs to ^{127}Cs. As is clearly seen in Fig. 8, the energy of the $g_{9/2}$ hole state increases with N. Because of the strongly upsloping character of this orbital the $g_{9/2}$ energy decreases with an increase in the β_2 deformation. However, the quadrupole deformation is decreasing with N leading to the observed systematics.

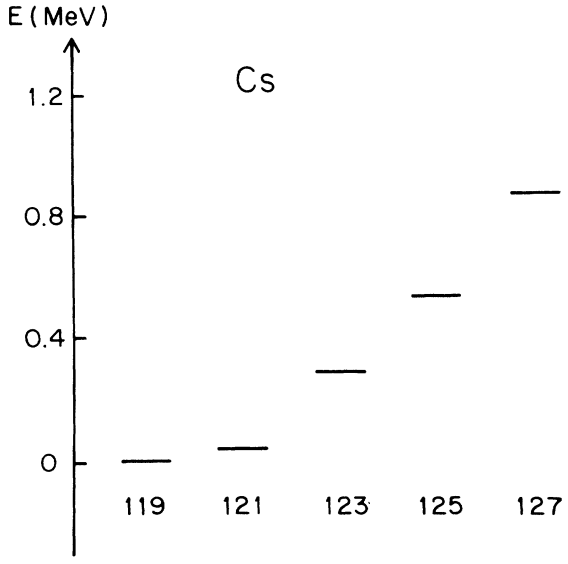

FIG. 8. Systematics of $g_{9/2}$ proton-hole states in odd-Z cesium isotopes.

C. Three-quasiparticle bands

Bands 1, 4, 6, and 8 are believed to be built on mixed proton-neutron three-quasiparticle configurations. The possible structures are discussed below.

1. Band 1

Band 1, built on a $\frac{13}{2}^-$ state, has been assigned a prolate $\pi g_{7/2}\otimes\nu h_{11/2}\otimes\nu g_{7/2}$ three-quasiparticle configuration following a comparison with two-quasineutron sidebands seen in neighboring even-even nuclei. Indeed, high-K sidebands built on the $\nu h_{11/2}\otimes\nu g_{7/2}$ configuration have systematically been observed in even-even xenon ($Z=54$) and barium ($Z=56$) isotopes, including the neighboring ^{126}Xe (Ref. 25) and ^{128}Ba (Ref. 26) isotones. These bands include the high-Ω $[404]\frac{7}{2}^+$ neutron orbital, from the top of the $\nu g_{7/2}$ shell, that is responsible for strong $\Delta I=1$ transitions and a lack of signature splitting in such bands. The bandheads of these low-lying $\nu h_{11/2}\otimes\nu g_{7/2}$ sidebands in the even nuclei are isomeric, with typical half-lives of a few ns, since these high-K ($K\sim5$) configurations can only decay into the $K=0$ ground-state bands.

In an odd-Z nucleus, this high-K two-quasineutron configuration would be coupled to the odd proton. Since, in the case of ^{127}Cs, the $\pi g_{7/2}$ orbital is lowest in energy, then the most likely choice for band 1 is the negative-parity $\pi g_{7/2}\otimes\nu h_{11/2}\otimes\nu g_{7/2}$ configuration. The high-K bandhead of this configuration would preferentially decay into other high-K states; indeed band 1 decays only into the high-K band 2, based on the $[404]\frac{9}{2}^+$ proton-hole orbital.

In the ^{129}La isotone,[27] a similar strongly-coupled sideband has been identified with the related positive-parity $\pi h_{11/2}\otimes\nu h_{11/2}\otimes\nu g_{7/2}$ configuration. However, in the lanthanum isotopes, the proton Fermi surface lies closer to the first $h_{11/2}$ proton orbital which explains the different configuration.

2. Band 8

Band 8, which decays into the yrast $\pi h_{11/2}$ band 7, shows two signature components with an energy splitting ($\sim$130 keV). Since the first $h_{11/2}$ proton crossing is blocked, band 8 is most likely based on the alignment of a pair of $h_{11/2}$ neutrons, namely the $\pi h_{11/2}\otimes[\nu h_{11/2}]^2$ configuration. The observed alignment $i_x\sim11\hbar$ is close to the sum of the alignments for the individual orbits of this configuration. For the favored signature, the extracted crossing frequency is $\hbar\omega_c=0.450(5)$ MeV, while a value of $\hbar\omega_c=0.425(5)$ MeV is obtained for the unfavored signature. For this band the observed $\Delta I=1$ $M1/E2$ transitions have similar intensities as the stretched $E2$ crossover transitions. The signature splitting reduces to half of that in band 7.

TRS calculations performed as a function of rotational frequency allow a comparison of the experimental obser-

vations with predictions for this rotational alignment. The results of these calculations for the favored $(-,-\frac{1}{2})$ $\pi h_{11/2}$ signature are shown in Fig. 6 for frequencies below and above the alignment of the $h_{11/2}$ neutron pair. The calculations predict a shape change from $(\beta_2=0.21,\gamma=+12°)$ below the alignment to $(\beta_2=0.18,\gamma=-23°)$ above the alignment. For the unfavored $(-,+\frac{1}{2})$ signature, the corresponding shapes are predicted to be $(\beta_2=0.21,\gamma=-7°)$ and $(\beta_2=0.20,\gamma=-43°)$, respectively. For both signatures, the shape change towards negative γ deformation is associated with the rotational alignment of an $h_{11/2}$ neutron pair. Such a shape change is expected because of the polarization effects of the upper-midshell $h_{11/2}$ neutrons on the γ-soft nuclear core. The decrease in the signature splitting associated with this alignment is consistent with the proposed shape change; the signature splitting for the $h_{11/2}$ proton orbital reaches its maximum at $\gamma\sim0°$ and decreases to near zero for $\gamma\sim-60°$. Band 8 still shows a signature splitting which indeed indicates a triaxial $(-60°<\gamma<0°)$ rather than an oblate $(\gamma=-60°)$ nuclear shape.

Furthermore, the TRS calculations predict the first unblocked $h_{11/2}$ proton crossing to occur at a relatively high frequency $\hbar\omega\sim0.7$ MeV. In addition, the calculations suggest that the $[\pi h_{11/2}]^3$ configuration terminates at an oblate shape $(\gamma=+60°)$. This region of frequency was not observed in the present experiment.

3. Band 6

The most probable configuration for band 6 is a $\pi g_{7/2}\otimes[\nu h_{11/2}]^2$ configuration, i.e., this band represents the $[h_{11/2}]^2$ neutron alignment for band 5 which is built on the two signatures of a $\pi g_{7/2}$ orbital. The alignments i_x of bands 5 and 6 are included in Fig. 5, while Fig. 6 shows TRS calculations for the favored $(+,-\frac{1}{2})$ $\pi g_{7/2}$ signature below and above the rotational alignment of the neutron pair. The calculations predict a shape change from $(\beta_2=0.20,\gamma=-3°)$ to $(\beta_2=0.17,\gamma=-37°)$ for both signatures following the neutron alignment. The shape change to negative γ deformation is similar to that predicted for the $[\nu h_{11/2}]^2$ alignment in the $\pi h_{11/2}$ band 7, but is larger because the strongly positive γ-driving $h_{11/2}$ orbital is not occupied. The crossing frequency extracted for the favored $(+,-\frac{1}{2})$ signature is $\hbar\omega_c=0.370(5)$ MeV, while $\hbar\omega_c=0.355(5)$ MeV is extracted for the unfavored $(+,+\frac{1}{2})$ signature. After the crossing, the signature splitting of band 6 is essentially zero.

It is difficult to explain the lack of signature splitting of band 6, especially with a predicted triaxial $(\gamma\sim-40°)$ shape. If, however, the shape was closer to the axially symmetric collective-oblate shape $(\gamma=-60°)$, then the $\pi g_{7/2}\otimes[\nu h_{11/2}]^2$ configuration would be dominated by the high-Ω $[404]\frac{7}{2}^+$ proton orbital, which would indeed lead to the strongly coupled nature of band 6 with no signature splitting. The $\frac{23}{2}^+$ bandhead of band 6 lies only 2 keV away from a state of the same spin and parity in band 5. No interaction between the two states seems to exist, indicating that these states are orthogonal to each other. This remarkably close proximity may indeed indicate a significant difference in the structure of these states, i.e., a prolate one-quasiproton state as compared to an oblate three-quasiparticle state.

Finally, an alternative structure that could explain the features of band 6, is the prolate $\pi h_{11/2}\otimes\nu h_{11/2}\otimes\nu g_{7/2}$ high-K configuration as seen in the ^{129}La isotone.[27] However, the bandhead spin $(\frac{23}{2}^+)$ of band 6 is probably too high to assign this configuration in ^{127}Cs; the present oblate $\pi g_{7/2}\otimes[\nu h_{11/2}]^2$ assignment is preferred.

4. Band 4

By comparison with band 6, band 4 is believed to represent the $[h_{11/2}]^2$ neutron alignment in the $\pi d_{5/2}$ band 3, and is thus built on the $\pi d_{5/2}\otimes[\nu h_{11/2}]^2$ configuration. The $B(M1)/B(E2)$ ratios observed for band 4 where the $E2$ crossovers were not observed are higher than those for band 6. Applying the model of Dönau and Frauendorf to both bands 4 and 6 at the same axially symmetric shape $(\gamma=-60°)$, this can be understood from the fact that the g factor for $\pi d_{5/2}$ is larger than that for $\pi g_{7/2}$, which enhances $M1$ transitions relatively. The crossing frequency extracted for the neutron alignment is $\hbar\omega_c=0.33$ MeV for band 4. The observed signature splitting is ~50 keV. The alignment of bands 4 and 6, included in Fig. 5, are similar.

When comparing the crossing frequencies for the $h_{11/2}$ neutron alignment in the band 3 to 4 ($\pi d_{5/2}$), band 5 to 6 ($\pi g_{7/2}$), and band 7 to 8 ($\pi h_{11/2}$), a systematic increasing is observed when going from the lower-j $d_{5/2}$ orbital to the higher-j $h_{11/2}$ orbital. This effect may reflect the stronger prolate polarizing effect of the higher-j orbital which hinders the alignment of the $h_{11/2}$ neutron pair.

In addition to a $[\nu h_{11/2}]^2$ alignment, $[\pi h_{11/2}]^2$ alignments are possible in bands 3 and 5. Such alignments have been observed in nearby lanthanum isotopes;[27,15] however, decoupled $\Delta I=2$ bands result in contrast to the strongly coupled bands 4 and 6.

IV. CONCLUSIONS

Several rotational bands have been established in ^{127}Cs. Low-spin bands built on $\pi h_{11/2}$, $\pi g_{7/2}$, and $\pi d_{5/2}$ orbitals are crossed by three-quasiparticle bands containing rotationally aligned $h_{11/2}$ neutrons. This neutron alignment is predicted to change the nuclear shape from near prolate $(\gamma\sim0°)$ to triaxial $(-60°\le\gamma\le0°)$. In addition, two strongly coupled prolate bands were observed. The first, built on the high-K $[404]\frac{9}{2}^+$ orbital, extends the systematics of $g_{9/2}$ proton-hole states seen in the light cesium isotopes. The second is related to the high-K $\nu h_{11/2}\otimes\nu g_{7/2}$ configurations seen in neighboring even-even nuclei. In ^{127}Cs, the lowest-energy proton orbital $(\pi g_{7/2})$ is coupled to this neutron configuration.

This work was in part supported by the National Science Foundation.

*Present address: Oliver Lodge Laboratory, University of Liverpool, P.O. Box 147, Liverpool L69 3BX, U.K.

[1]E. S. Paul, C. W. Beausang, D. B. Fossan, R. Ma, W. F. Piel, Jr., N. Xu, L. Hildingsson, and G. A. Leander, Phys. Rev. Lett. **58**, 984 (1987), and references therein.

[2]G. A. Leander, S. Frauendorf, and F. R. May, in *Proceedings of the Conference on High Angular Momentum Properties of Nuclei, Oak Ridge, 1982,* edited by N. R. Johnson (Harwood Academic, New York, 1983), p. 281.

[3]S. Frauendorf and F. R. May, Phys. Lett. **125B**, 245 (1983).

[4]I. Ragnarsson, A. Sobiczewski, R. K. Sheline, S. E. Larsson, and B. Nerlo-Pomorska, Nucl. Phys. **A233**, 329 (1974).

[5]Y. S. Chen, S. Frauendorf, and G. A. Leander, Phys. Rev. C **28**, 2437 (1983).

[6]G. Andersson, S. E. Larsson, G. Leander, P. Möller, S. G. Nilsson, I. Ragnarsson, S. Åberg, R. Bengtsson, J. Dudek, B. Nerlo-Pomorska, K. Pomorski, and Z. Szymański, Nucl. Phys. **A268**, 205 (1976).

[7]R. Wyss, A. Johnson, J. Nyberg, R. Bengtsson, and W. Nazarewicz, Z. Phys. A **329**, 255 (1988).

[8]G. Beyer, A. Jasiński, O. Knotek, H. -G. Ortlepp, H. -U. Siebert, R. Arlt, E. Herrmann, G. Musiol, and H. Tyrroff, Nucl. Phys. **A260**, 269 (1976).

[9]U. Garg, T. P. Sjoreen, and D. B. Fossan, Phys. Rev. C **19**, 207 (1979).

[10]R. Wyss, J. Nyberg, A. Johnson, R. Bengtsson, and W. Nazarewicz, Phys. Lett. B **215**, 211 (1988).

[11]L. Hildingsson, C. W. Beausang, D. B. Fossan, W. F. Piel, Jr., A. P. Byrne, and G. D. Dracoulis, Nucl. Instrum. Methods **A252**, 91 (1986).

[12]K. S. Krane, R. M. Steffen, and R. M. Wheeler, Nucl. Data Tables **A11**, 351 (1973).

[13]T. Yamazaki, Nucl. Data **A3**, 1 (1967).

[14]R. D. Gill, *Gamma-ray Angular Correlations* (Academic, New York, 1975), p. 180.

[15]L. Hildingsson, C. W. Beausang, D. B. Fossan, R. Ma, E. S. Paul, W. F. Piel, Jr., and N. Xu, Phys. Rev. C **39**, 471 (1989).

[16]L. Hildingsson, C. W. Beausang, D. B. Fossan, and W. F. Piel, Jr., Phys. Rev. C **37**, 985 (1988).

[17]T. M. Semkow, D. G. Sarantites, K. Honkanen, V. Abenante, L. A. Adler, C. Baktash, N. R. Johnson, I. Y. Lee, M. Oshima, Y. Schutz, Y. S. Chen, J. X. Saladin, C. Y. Chen, O. Dietzsch, A. J. Larabee, L. L. Riedinger, and H. C. Griffin, Phys. Rev. C **34**, 523 (1986).

[18]T. W. Conlon, Nucl. Phys. **A161**, 289 (1971).

[19]U. Garg, T. P. Sjoreen, and D. B. Fossan, Phys. Rev. C **19**, 217 (1979).

[20]R. Bengtsson and S. Frauendorf, Nucl. Phys. **A327**, 139 (1979).

[21]S. M. Harris, Phys. Rev. **138**, B509 (1965).

[22]W. Nazarewicz, J. Dudek, R. Bengtsson, T. Bengtsson, and I. Ragnarsson, Nucl. Phys. **A435**, 397 (1985).

[23]F. Dönau and S. Frauendorf, in *Proceedings of the Conference on High Angular Momentum Properties of Nuclei, Oak Ridge, 1982,* edited by N. R. Johnson (Harwood Academic, New York, 1983), p. 143; F. Dönau, Nucl. Phys. **A471**, 469 (1987).

[24]A. J. Larabee, L. H. Courtney, S. Frauendorf, L. L. Riedinger, J. C. Waddington, M. P. Fewell, N. R. Johnson, I. Y. Lee, and F. K. McGowan, Phys. Rev. C **29**, 1934 (1984).

[25]W. Lieberz, S. Freund, A. Granderath, A. Gelberg, A. Dewald, R. Reinhardt, R. Wirowski, K. O. Zell, and P. von Brentano, Z. Phys. A **330**, 221 (1988).

[26]K. Schiffer, A. Dewald, A. Gelberg, R. Reinhardt, K. O. Zell, Sun Xianfu, and P. von Brentano, Nucl. Phys. **A458**, 337 (1986).

[27]Y. He, M. J. Godfrey, A. J. Kirwan, P. J. Nolan, D. J. Thornley, S. M. Mullins, and R. Wadsworth, University of Liverpool Nuclear Structure Group Annual Report, 1988, p. 16.

[28]W. F. Piel, Jr., P. Chowdhury, U. Garg, M. A. Quadar, P. M. Swertka, S. Vajda, and D. B. Fossan, Phys. Rev. C **31**, 456 (1985).

[29]R. E. Shroy, D. M. Gordon, M. Gai, D. B. Fossan, and A. K. Gaigalas, Phys. Rev. C **26**, 1089 (1982).